ORIENTAL JOURNAL OF CHEMISTRY
An International Open Access, Peer Reviewed Research Journal
www.orientjchem.org
ISSN: 0970-020 X
CODEN: OJCHEG
2025, Vol. 41, No.(4):
Pg. 1255-1268

Molecular Docking Studies and *In silico* ADMET Screening of New Chalcones as Lanosterol α-Demethylase and DNA Gyrase Topoisomerase B Inhibitors

AKHLESH KUMARI[1]* and SUSHIL KUMAR[2]

[1,2]School of Pharmaceutical Sciences, Faculty of Pharmacy, IFTM University, Moradabad-244102 (U.P.), India.
*Corresponding author E-mail: akhigangwar1991@gmail.com

http://dx.doi.org/10.13005/ojc/410422

(Received: March 11, 2025; Accepted: July 17, 2025)

ABSTRACT

Chalcone and their benzotriazole derivatives originate from the nucleus ability to interpose into DNA base pairs, which inhibit lanosterol α-demethylase and DNA gyrase topoisomerase B. The active sites of topoisomerase B and lanosterol are the sites of molecular docking studies that provide comprehension of the intermolecular interactions for antimicrobial activity. Docking and ADMET properties of designed substituted benzaldehyde chalcones and their benzotriazoles using Schrodinger suit-2024 Maestro and SwissADME software programs against lanosterol α-demethylase and DNA gyrase topoisomerase B. *C. albicans* (lanosterol α-demethylase, PDB ID:4WMZ) and *E. coli* (DNA gyrase topoisomerase B, PDB ID:1KZN) were selected for their respective binding affinities based on interaction patterns, GLIDE scores and docking scores. Compounds (7B1-7B7 and 9B1-9B3) showed strong binding interactions, and their ability to inhibit lanosterol α-demethylase (4WMZ) and DNA gyrase topoisomerase B (1KZN) for antimicrobial activity. Among the compounds, 9B1, 9B2, 9B3, and 7B1 have good binding affinity with GLIDE scores in the range of -10.655 to -10.154 against *C. albicans* and 7B1, 7B2 and 9B2 have good binding affinity with GLIDE score in range of -5.613 to -5.083 against E. coli when compared with the standard Fluconazole (-6.58) and Amoxicillin (-5.29). Test compounds showed good ADMET properties and similarity with respect to standard drugs. Molecular docking studies and in silico ADMET screening of new chalcones and their benzotriazole derivatives could be used as inhibitors of lanosterol α-demethylase (4WMZ) and DNA gyrase topoisomerase B (1KZN). Additional *in-vitro* and *in-vivo* research could confirm its potential as antimicrobials.

Keywords: DNA gyrase B, Lanosterol α-demethylase, Borneol, Chalcones, Antimicrobials, Docking studies, *In-silico* ADMET, Percentage Similarity.

INTRODUCTION

Chalcones, first identified during flavonoid biosynthesis, possess an α-β unsaturated carbonyl system linking two aromatic rings, a structure that is crucial for their biological activity[1]. These compounds, abundant in medicinal plants, belong to the flavonoid and isoflavonoid (terpenoids) families and exhibit a wide range of biological activities, including antibacterial, antifungal, anti-inflammatory, antioxidant and anticancer properties[2]. Chalcone derivatives work by blocking the lanosterol

α-demethylase and DNA gyrase topoisomerase B[3,4]. Their high activity resulted from the chalcone containing benzotriazole nucleus ability to intercalate into DNA base pairs, stabilizing the cleavable complex of lanosterol and topoisomerase B and producing the ternary complex[5]. This is a DNA interpolating agent to be identified as a lanosterol and topoisomerase B inhibitor[6]. In compounds with a sufficiently enormous coplanar aromatic chromophore, the strongest form of reversible binding to the double helix DNA is the intercalation process[7,8]. A major factor in the cytotoxicity of most clinically effective DNA-intercalating medications is their blocking of lanosterol and DNA-topoisomerase B[9]. According to several detailed SAR studies of chalcone-based DNA-interpolating agents[10]. When adding different substitutions on chalcones and including benzotriazole, researchers were able to expand their study of the structure-activity relationship and gain a new understanding of molecular interactions at the receptor site. It is well-established that the tiniest structural changes to chalcones can have a variety of pharmacological effects. similarly, benzotriazole-based chalcone derivatives exhibit a range of biological activities, including antibacterial and antifungal properties[11,12]. We have developed benzaldehyde-substituted chalcone analogs and their benzotriazoles for lanosterol and topoisomerase B inhibition through molecular docking studies using the Schrodinger Maestro suite 2024-1 (Schrodinger, LLC, New York, NY) software. continuing our earlier research work,7B1-7B7 and 9B1-9B3 on finding new influential antimicrobial agents[13]. In this work, newly designed chalcones and their benzotriazoles will be explored using molecular docking against lanosterol α-demethylase and DNA gyrase topoisomerase B as antimicrobials. The designed compounds exhibited good in silico SWISSADME characteristics and similarity parameters when compared with respective standard drugs.

MATERIALS AND METHODS

Protein preparation

During the optimization process, the active sites of *C. albicans* lanosterol α-demethylase (PDB ID:4WMZ) and E. coli DNA gyrase topoisomerase B (PDB ID: 1KZN) were downloaded from RCSB protein data bank (https://www.rcsb.org/docs/3d-viewers/mol) and utilized in molecular docking of strong antifungal (fluconazole) and antibacterial (amoxicillin) drugs. All structures were optimized before docking using the protein preparation wizard, Schrodinger Suite 2024-1 software. The amino acid numbers and crystal structures are identical. Protein structures are typically revised based on their topologies, incomplete terminal groups, missing hydrogen atoms, bond orders, and formal charges. Beyond the heteroatom, water molecules were removed. The most stable of the probable ionization states produced for the heteroatom found in the protein structure was chosen. Orientations of retained water molecules were adjusted, and hydrogen bonds were allocated. This phase involved assigning the bond order, adding the hydrogen in the structure, deleting the bond to the metal, adjusting the formal charge on the metal and its nearby atoms, and deleting those water molecules that were closer than 5 Å specified distance. It produces the Het state option, which predicts ionization and the tautomer state of the Het group at pH 6.5 to 7.2. The hydrogen bond network optimization was the next step in the protein preparation process. The structure must be refined with a limited minimization at the last stage of preparation. Their task is initiated in the improved Minimization for the (optimized potential for liquid simulation) OPLS-2005 force field minimization with a 0.3 Å RMSD.

Ligand preparation

The program Chem Draw Ultra version 12.0 was used to generate the ligand structures in the CDX format. After that, ligands were converted to mol2 format and processed by the Schrodinger Maestro Suite 2024-1 LigPrep part. LigPrep tool (LigPrep, Schrodinger, LLC software) was used to prepare the ligand structures before docking. They were desalted, chirality and deficient hydrogen atom modifications were created, and their shape was optimized. Stereochemical, ionization and tautomeric variants were also included, along with energy minimization and conversion from 2D to 3D structures. Their bond arrangement was established when the charged groups of these ligands were neutralized. Each ligand produced a single low-energy ring confirmation and docking analysis was performed using the optimized ligands.

Receptor grid generation

Glide explores the optimal form and orientation for interactions between macromolecules and micromolecules. The generated protein crystal

structure retained the ligand (chalcone derivatives), which was utilized in creating the receptor grid. The Schrodinger tool was used to create grid boxes surrounding the protein binding area that were 40 × 40 × 40 Å3 in dimensions and spaced 0.375 Å apart.

Validation of the docking protocol

According to the object scoring function, the extent to which the co-crystallized ligand's lowest energy pose (binding conformation) an experimental binding mode revealed by X-ray crystallography, was mimicked by the glide score, which was used to evaluate the docking process accuracy. Additional accuracy in removing co-crystallized ligand from protein binding site and redocking the ligand with its binding site allowed the Glide docking process to be validated. Root mean square deviation (RMSD) between the predicted confirmation and the measured X-ray crystallographic form was used to interpret the data, along with the hydrogen bond interactions. The docking method was validated when the tested and standard drug conformations were compared. The low RMSD of 2.9 Å (1KZN) and 1.8 Å (4WMZ) showed that the conformations were comparable.

Ligand docking using Glide

The ligand molecules and previously created receptor grid were used to perform the Glide docking of the proposed compounds[14]. To determine the interactions between ligand molecules and the receptor, the Glide ligand docking tool was utilized.[15] Docking calculations were performed using the extra precision and force field modes of the OPLS-2005[16]. Flexibility docking mode was used for the docking process, which automatically generates conformations for each input ligand. A collection of hierarchical filters was applied to the ligand-receptor poses that were produced to assess the ligand-receptor interaction. The first filter tests the ligand's spatial fit to the assigned active site and investigates the complementarity of ligand-receptor interactions using a grid-based approach centered on the empirical ChemScore function. This technique penalizes steric incompatibilities while identifying advantageous hydrogen and hydrophobic bonding. The poses proceed to the last stage of the algorithm, which involves assessing and minimizing a grid approximation, after passing the first screens. Subsequently, the Glide Score scoring algorithm was used to re-score the minimized poses. All ligand's fitness scores in lanosterol and topoisomerase B were compared, and the active compounds' Glide scores were compiled. Most of the proposed compounds have good Glide scores when compared to the Glide scores of standard drugs that consist of substituted benzaldehyde chalcone and their benzotriazole derivatives, which are utilized as antimicrobial agents, as well as strong lanosterol and topoisomerase B.

ADMET Prediction

Following a detailed description of each synthesized compound, software analysis was performed on the test compounds[17]. To compile information about ADMET, the parameters of common drugs (Amoxicillin, Norfloxacin, and Fluconazole) and compounds ($7B_1$-$7B_7$ and $9B_1$-$9B_3$) were calculated using the SwissADME online web-based tool (http://www.swissadme.ch/;last), Molinspiration (https://www.molinspiration.com), and Osiris property explorer (http://www.organicchemistry.org/prog/peo/) software programs. These parameters included their physicochemical, lipophilicity, water solubility, pharmacokinetics, drug resemblance, and medicinal chemistry[18,19]. After that, the similarity of test compounds to standard drugs was calculated and analysed by their physicochemical characteristics[20,21].

RESULTS AND DISCUSSION

Molecular Docking

Docking studies are now considered a crucial part of drug development in the context of in-silico investigations[22]. Glide was used for the docking, while Prime was used to calculate the binding energy[23]. The ligands were docked to protein active sites using Schrodinger Maestro Suite 2024, a complex molecular docking database, to ascertain the compounds' binding affinities[24]. To determine their lanosterol α-demethylase and DNA gyrase topoisomerase B inhibitory ability, the developed analogues are docked towards the *C. albicans* (lanosterol α-demethylase, 4WMZ) and *E. coli* (DNA gyrase topoisomerase B, 1KZN). Among the compounds, $9B_1$, $9B_2$, $9B_3$, and $7B_1$ have good binding affinity with GLIDE scores in the range of -10.655 to -10.154 against *C. albicans* and $7B_1$, 7B2 and 9B2 showed good binding affinity with GLIDE score in range of -5.613 to -5.083 against *E. coli* when compared with standard Fluconazole

(-6.58) and Amoxicillin (-5.29). Docking results of the two most potent compounds 9B3 and 7B1 are presented in Tables 1 & 2, revealing diverse interactions with the active site of chlorobiocin and fluconazole (endogenous ligands). The binding mode and various types of interactions observed for 9B3 and 7B1 are shown in Fig. 1 & 4, respectively. The active site of PBP-lanosterol αdemethylase of *C. albicans* (fluconazole), consists of amino acid residues Tyr126, Tyr140, Lys150, His378, Leu380, Arg385, Pro462, Phe463, Gly464, His468 and Cys470 and PBP-DNA gyrase topoisomerase B of *E. coli* & *S. aureus* (chlorobiocin), consists of amino acid residues Asn46, Glu50, Arg76, Gly77, Ile78, Pro79, Ile90, Val93, Ala96, Gly119, Val120, Ser121. This is where PBP-DNA gyrase inhibitors bind, then exert their bactericidal activity. According to the results of the binding model, compounds 9B3 and 7B1 interact with the same active site as chalcone analogues and other inhibitors that have been previously described by utilising a combination of van der Waals, hydrophobic, electrostatic, covalent, and H-bonding interactions. Additionally, 23 amino acid residues, e.g., Leu95, Tyr126, Lys151, Leu158, Val154, Phe236, Pro238, Phe241, Val311, Gly314, Gly315, Leu380, Hie381, Ser382, Leu383, Phe384, Cys470, Gly472, Phe506, Thr507, Ser508, Met509, Val510 were involved in van de Waals interactions to stabilize the 9B3-PBP-4WMZ receptor complex. Since *Candida albicans* is known to be both hydrophilic and hydrophobic, both 9B3 and 7B1 showed notable hydrophobic interactions with specific receptor residues surrounding the α, β-unsaturated carbonyl moiety and phenyl ring A. For 7B1, these residues included Val43, Asn46, Ala47, Val71, Gln72, Asp73, Arg76, Pro79, Ala86, Val89, Ile90, Ala96, Val120, Thr165, Met166 and Val167. Interactions between protein and ligand of effective analogs ($9B_3$, $9B_2$, and $7B_1$) against lanosterol α-demethylase (PDB-ID, 4WMZ) are shown in Fig. 1-4, and $7B_1$, $9B_2$, and $7B_2$ against DNA gyrase topoisomerase B (PDB-ID, 1KZN) are shown in Fig. 5-8. Structure and name of designed compounds $7B_1$-$7B_7$ and $9B_1$-$9B_3$ using ChemDraw Ultra version 12.0, included in Figures 9 and 10.

Table 1: Docking studies of new chalcones against lanosterol α-demethylase (4WMZ)

Compounds	Glide score	Glide energy kcal/mol	Interacting ligand-protein amino acid residues
7B1	-10.154	-78.158	Tyr72, Gly73, Leu95, Leu96, Arg98, Tyr126, Ile129, Phe134, Ile139, Pro238, Phe241, Val242, Gly314, Leu380, Hie381, Ser382, Leu383, Phe384, Phe506, Thr507, Ser508, Met509, Val510
7B2	-9.874	-70.538	Gly73, Leu95, Leu96, Arg98, Tyr126, Ile129, Thr130, Phe134, Phe236, Phe241, Val242, Gly314, Thr318, Ser382, Leu383, Phe384, Phe506, Thr507, Ser508, Met50
7B3	-8.059	-59.223	Tyr72, Leu95, Arg98, Tyr126, Ile129, Thr130, Phe134, Tyr140, Pro238, Phe241, Val242, Gly314, Thr318, Leu380, Hie381, Ser382, Leu383, Phe384, Phe506, Thr507, Met509, Val510.
7B4	-7.692	-60.174	Tyr72, Gly73, Leu96, Arg98, Tyr126, Ile139, Tyr140, Phe236, Pro238, Phe241, Gly314, Thr318, Hie381, Ser382, Leu383, Phe384, Phe506, Thr507, Met509, Val510.
7B5	-8.75	-67.422	Tyr72, Tyr126, Thr130, Phe134, Ile139, Tyr140, Phe241, Gly314, Thr318, Leu380, Hie381, Ser382, Leu383, Phe384, Phe506, Thr507, Ser508, Val510.
7B6	-8.275	-62.585	Tyr72, Gly73, Leu95, Leu96, Arg98, Tyr126, Ile129, Thr130, Phe134, Pro238, Gly314, Thr318, Leu380, Hie381, Ser382, Leu383, Phe384, Phe506, Thr507, Ser508.
7B7	-8.112	-58.108	Gly73, Leu95, Leu96, Arg98, Tyr126, Phe134, Tyr140, Phe236, Phe241, Val242, Gly314, Thr318, Leu380, Hie381, Ser382, Leu383, Phe506, Ser508, Met509, Val510.
9B1	-10.455	-78.158	Tyr126, Leu129, Tyr140, Val154, Phe236, Val311, Gly315, Thr318, Ser319, Thr322, Ile339, Leu374, Leu380, Hie378, Pro379, Leu383, Pro462, Phe463, Gly462, His468, Cys470, Ile471, Gly472, Phe475, Ala476, Phe506, Met509, Val510.
9B2	-10.523	-82.026	Tyr72, Gly73, Leu95, Tyr126, Leu129, Thr130, Phe134, Tyr140, Lys151, Leu158, Val154, Pro238, Phe241, Val311, Gly314, Gly315, Leu380, Hie381, Ser382, Leu383, Gly472, Phe506, Thr507, Ser508, Met509, Val510.
9B3	-10.655	89.245	Leu95, Tyr126, Lys151, Leu158, Val154, Phe236, Pro238, Phe241, Val311, Gly314, Gly315, Leu380, Hie381, Ser382, Leu383, Phe384, Cys470, Gly472, Phe506, Thr507, Ser508, Met509, Val510.
Fluconazole	-6.58	-52.065	Tyr126, Tyr140, Lys150, His378, Leu380, Leu383, Arg385, Pro462, Phe463, Gly464, His468, Cys470.

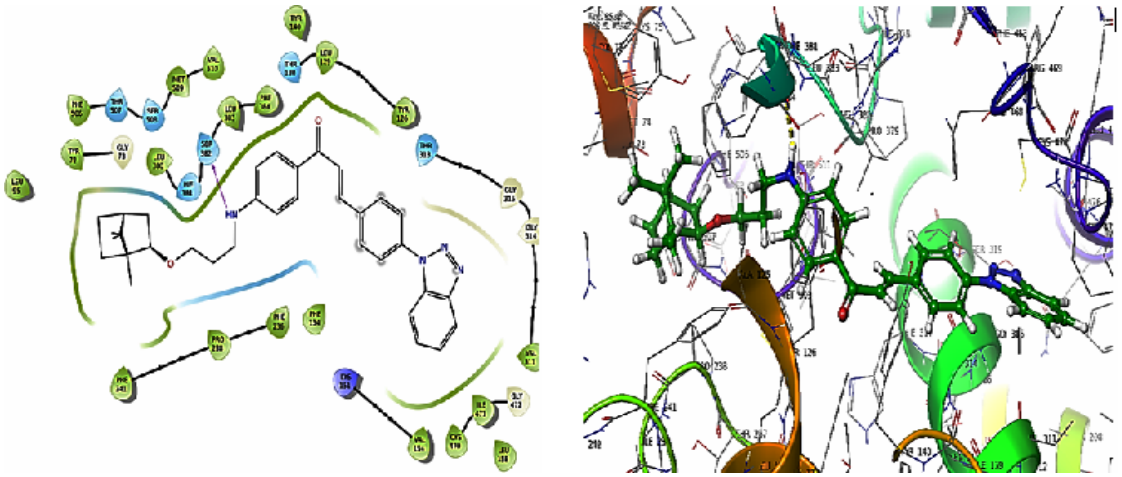

Fig. 1. Interactions between protein and ligand of more potent analogue $9B_3$ against 4WMZ using Schrodinger Maestro Suite 2024-1 (Source: Schrodinger, LLC, New York, NY)

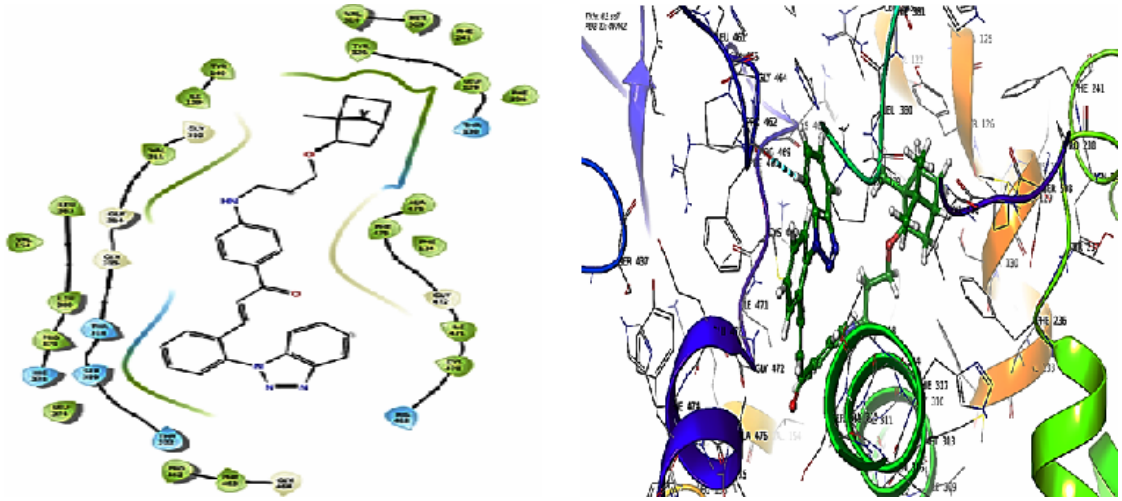

Fig. 2. Interactions between protein and ligand of the more potent analogue $9B_2$ against 4WMZ

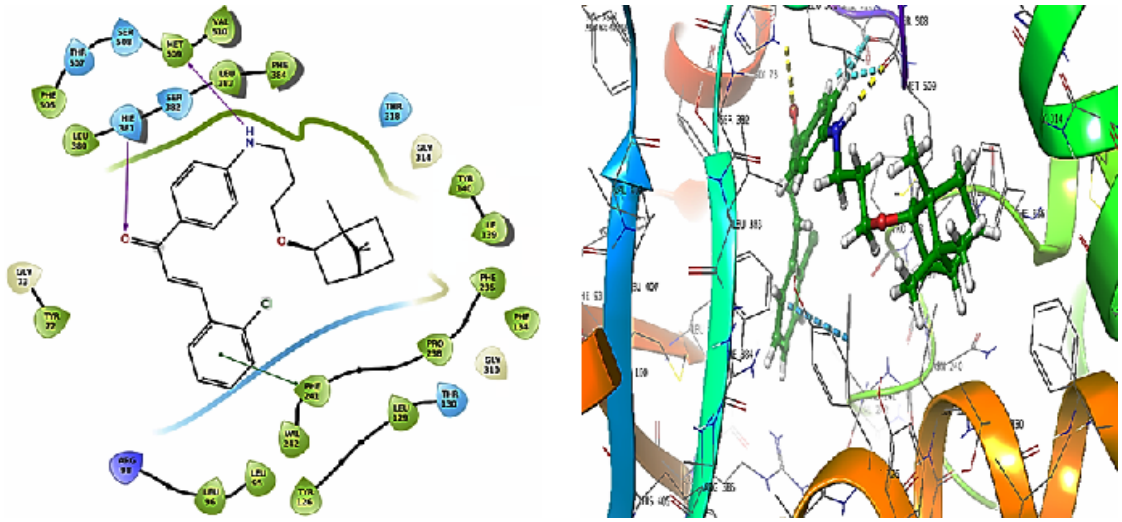

Fig. 3. Interactions between the protein and ligand of the more potent analogue $7B_1$ against 4WMZ

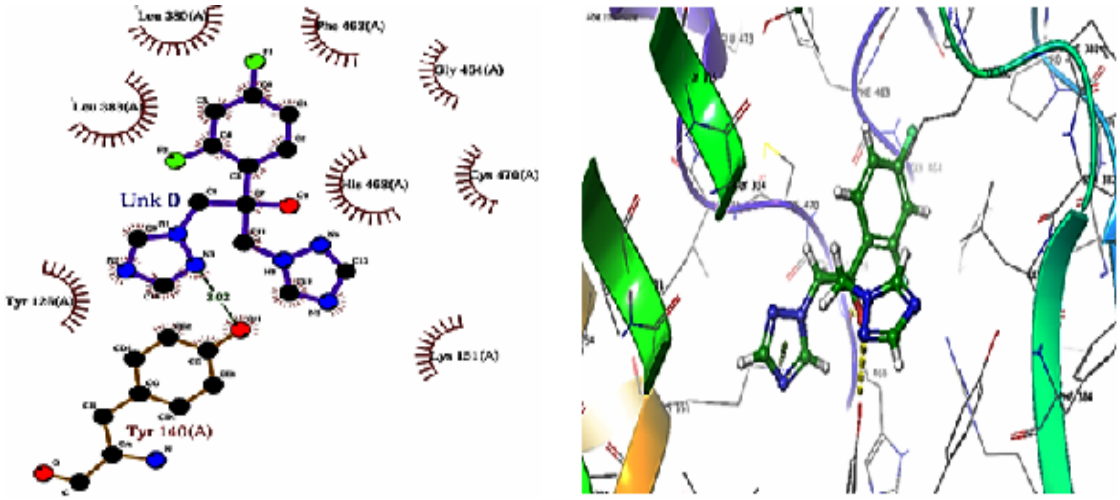

Fig. 4. Interactions between protein and standard fluconazole against 4WMZ

Table 2: Docking studies of new chalcones against topoisomerase B (1KZN)

Compounds	Glide score	Glide energy kcal/mol	Interacting ligand-protein amino acid residues
7B1	-5.613	-46.899	Val43, Asn46, Ala47, Val71, Gln72, Asp73, Arg76, Pro79, Ala86, Val89, Ile90, Ala96, Val120, Thr165, Met166, Val167.
7B2	-5.352	-51.00	Val43, Asn46, Asp49, Glu50, Gln72, Asp73, Arg76, Ile78, Ala86, Val89, Ile90, Ala96, Val120, Thr165, Met166, Val167.
7B3	-4.58	-47.246	Ala47, Asp49, Glu50, Val71, Gln72, Asp73, Arg76, Ile78, Pro79, Ala86, Val89, Ile90, Ala96, Val120, Thr165, Met166, Val167.
7B4	-4.789	-48.539	Val43, Asn46, Ala47, Glu50, Val71, Gln72, Asp73, Arg76, Ile78, Pro79, Ala86, Val89, Ile90, Val120, Thr165, Met166, Val167.
7B5	-3.074	-33.519	Asn46, Val43, Asn46, Ala47, Asp49, Glu50, Val71, Gln72, Asp73, Arg76, Ile78, Pro79, Val89, Ile90, Ala96, Thr165, Met166.
7B6	-3.469	-40.469	Val43, Asn46, Ala47, Asp49, Glu50, Val71, Gln72, Asp73, Arg76, Ile78, Pro79, Ile90, Ala96, Val120, Thr165, Met166, Val167.
7B7	-4.675	-32.083	Val43, Asp49, Glu50, Val71, Gln72, Asp73, Arg76, Ile78, Pro79, Ala86, Val89, Ile90, Ala96, Val120, Thr165, Val167.
9B1	-4.519	-51.00	Glu50, Val71, Asp73, Arg76, Ile78, Pro79, Gly81, Ile82, Val84, Ser85, Ala86, Val89, Met91, Ala96, Val120, Thr165, Val167.
9B2	-5.083	-58.714	Val43, Asn46, Ala47, Glu50, Val71, Asp72, Asp73, Arg76, Ile78, Gly81, Ile82, Val84, Ser85, Ala86, Ile90, Met91.Ala96, Val120, Thr165, Val167.
9B3	-4.724	-48.399	Val43, Ala47, Glu50, Val71, Asp72, Asp73, Arg76, Ile78, Pro79, Gly81, Ile82, Ser85, Ala86, Val89, Val120, Thr165.
Amoxicillin	-5.29	-49.092	Asn46, Glu50, Arg76, Gly77, Ile78, Pro79, Ile90, Val93, Ala96, Gly119, Val120, Ser121.S

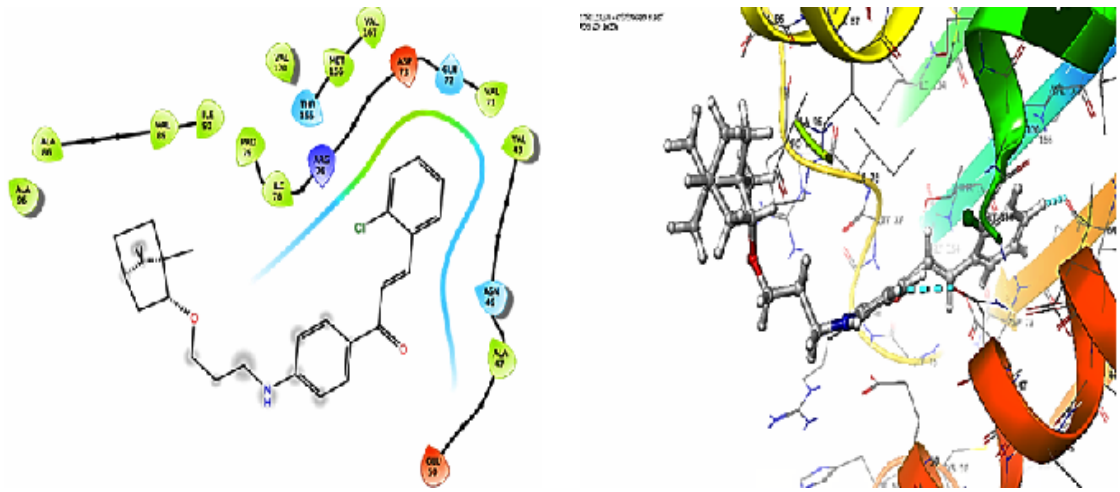

Fig. 5. Interactions between protein and ligand of the more potent analogue 7B$_1$ against 1KZN

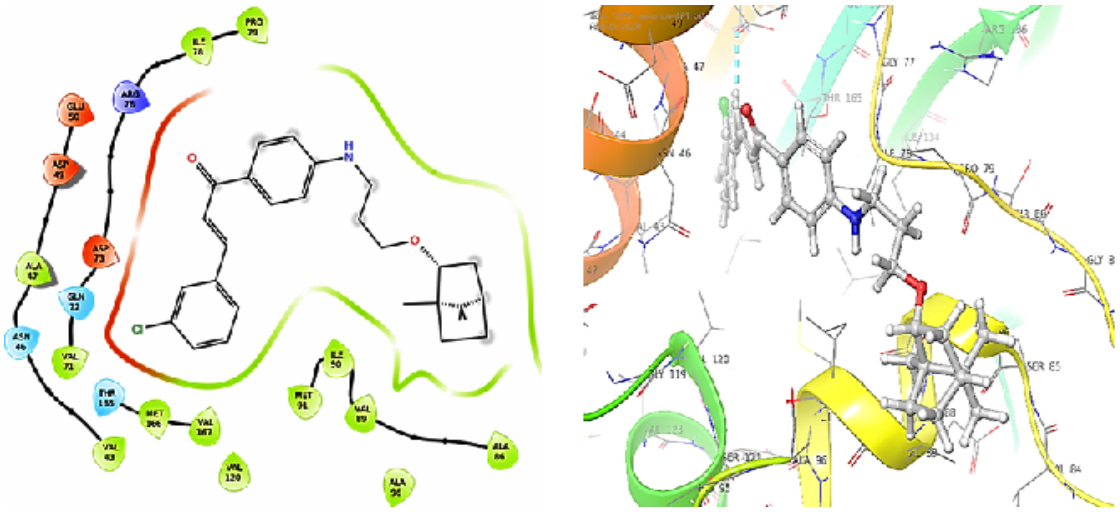

Fig. 6. Interactions between protein and ligand of the more potent analogue $7B_2$ against 1KZN

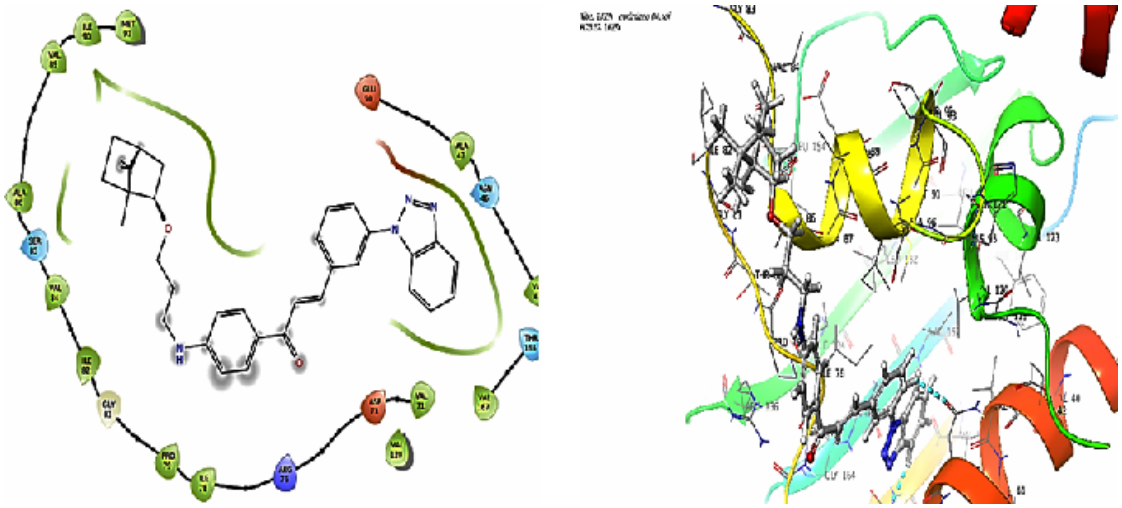

Fig. 7. Interactions between protein and ligand of the more potent analogue $9B_2$ against 1KZN

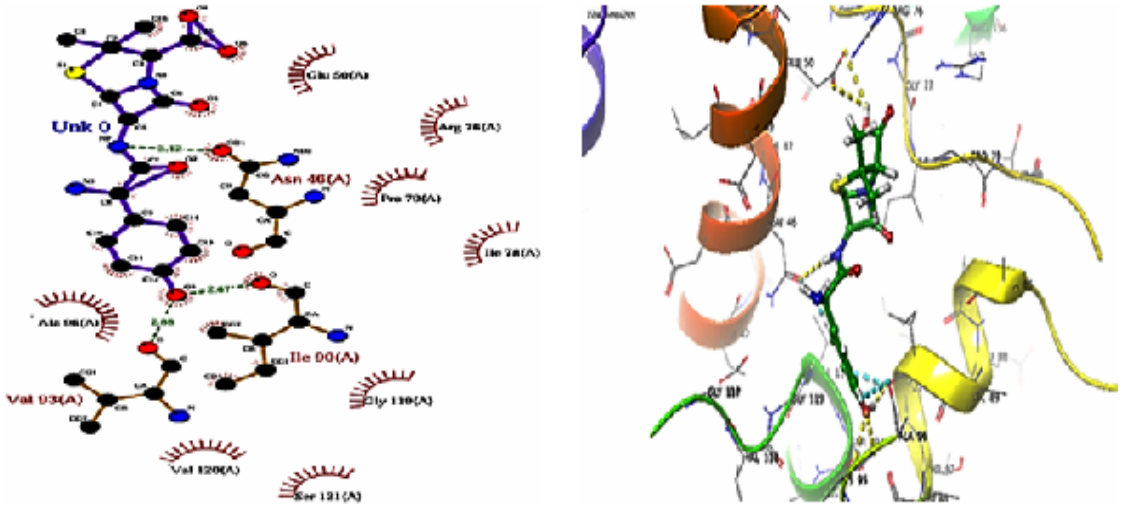

Fig. 8. Interactions between protein and standard Amoxicillin against 1KZN

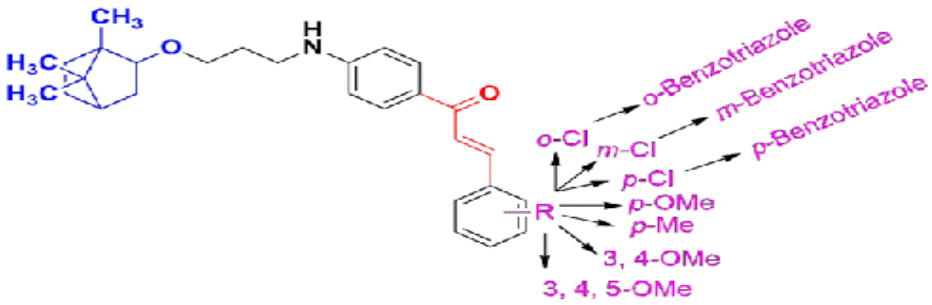

Fig. 9. Structure of designed chalcones $7B_1$-$7B_7$ and $9B_1$-$9B_3$ using ChemDraw Ultra version 12.0

$7B_1$

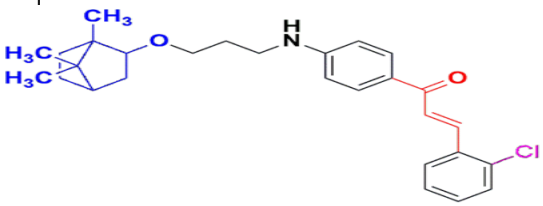

(E)-3-(2-chlorophenyl)-1-(4-(3-(1,7,7-trimethylbicyclo [2.2.1] heptan-2-yl) oxy) propyl) amino) phenyl) prop-2-en-1-one

$7B_2$

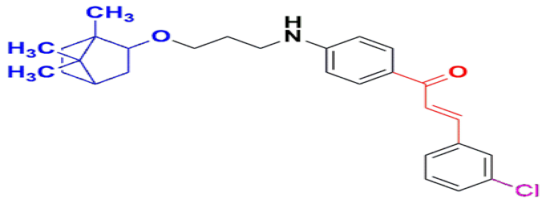

(E)-3-(3-chlorophenyl)-1-(4-(3-(1,7,7-trimethylbicyclo [2.2.1] heptan-2-yl) oxy) propyl) amino) phenyl) prop-2-en-1-one

$7B_3$

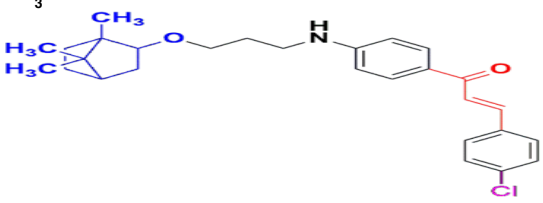

(E)-3-(4-chlorophenyl)-1-(4-(3-(1,7,7-trimethylbicyclo [2.2.1] heptan-2-yl) oxy) propyl) amino) phenyl) prop-2-en-1-one

$7B_4$

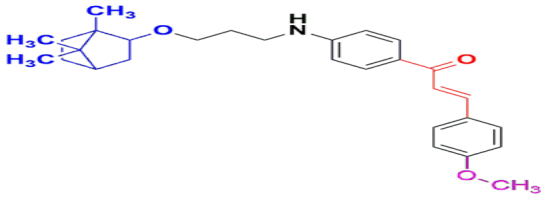

(E)-3-(4-methoxyphenyl)-1-(4-(3-(1,7,7-trimethylbicyclo [2.2.1] heptan-2-yl) oxy) propyl) amino) phenyl) prop-2-en-1-one

$7B_5$

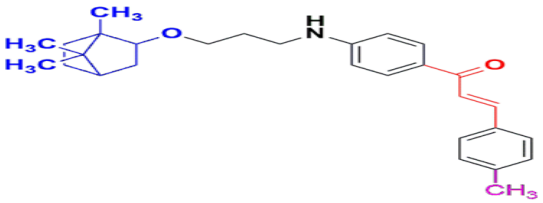

(E)-3-(p-tolyl)-1-(4-((3-((1,7,7-trimethylbicyclo [2.2.1] heptan-2-yl) oxy) propyl) amino) phenyl) prop-2-en-1-one

$7B_6$

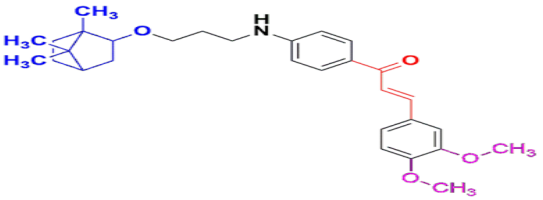

(E)-3-(3,4-dimethoxyphenyl)-1-(4-(3-(1,7,7-trimethylbicyclo [2.2.1] heptan-2-yl) oxy) propyl) amino) phenyl) prop-2-en-1-one

$7B_7$

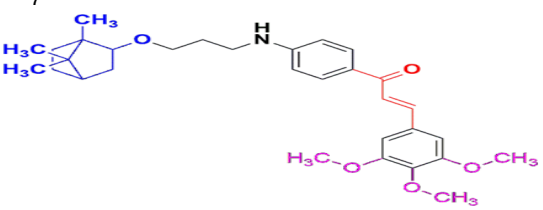

(E)-3-(3,4,5-trimethoxyphenyl)-1-(4-((3-((1,7,7-trimethylbicyclo [2.2.1] heptan-2-yl) oxy) propyl) amino) phenyl) prop-2-en-1-one

$9B_1$

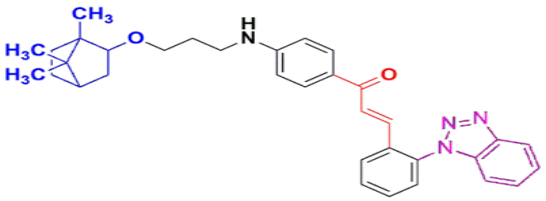

(E)-3-(2-(1H-benzo[d] [1,2,3] triazol-1-yl) phenyl)-1-(4-(3-((1,7, 7-trimethylbicyclo [2.2.1] heptan-2-yl) oxy) propyl) amino) phenyl) prop-2-en-1-one

$9B_2$

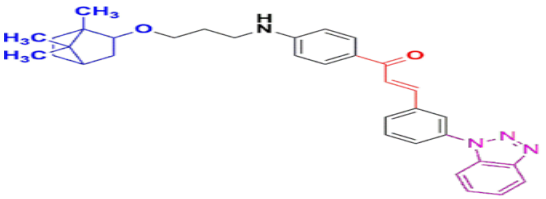

(E)-3-(3-(1H-benzo[d][1,2,3] triazol-1-yl) phenyl)-1-(4-(3-(1, 7, 7-trimethylbicyclo [2.2.1] heptan-2-yl) oxy) propyl) amino) phenyl) prop-2-en-1-one

$9B_3$

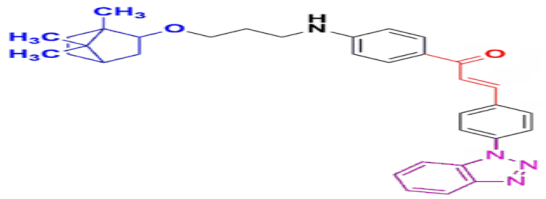

(E)-3-(4-(1H-benzo[d] [1,2,3] triazol-1-yl) phenyl)-1-(4-(3-((1,7,7-trimethylbicyclo [2.2.1] heptan-2-yl) oxy) propyl) amino) phenyl) prop-2-en-1-one

Fig. 10. Structure and name of designed compounds $7B_1$-$7B_7$ and $9B_1$-$9B_3$ using ChemDraw Ultra version 12.0

Prediction of absorption, distribution, metabolism, excretion and toxicity

Physicochemical, pharmacokinetic (ADMET) properties were estimated by using "SwissADME, Molinspiration and Osiris property explorer". The results obtained are summarised in Tables 3 and 4. According to Lipinski's Rule of Five, compounds are likely to have good oral bioavailability if they satisfy the various parameters like molecular weight (MW), partition coefficient (log p), Hydrogen bond donors (HBD), Hydrogen bond acceptors (HBA) and Total Polar Surface Area (TPSA). The predicted analysis revealed that designed chalcones $7B_4$, $7B_5$ and $7B_6$ except good physicochemical properties, while compound 7B4 showed a violation of Lipinski's rule of five. The molecular weight of test compounds is between 447.61-534.69 gm/mol. MW represents the total mass of a molecule; if it is less than 500, it indicates a compound that is sufficiently large to interact with biological targets. According to the formula stated (% Abs =109 [0.345 ×TPSA]), the percentage of absorption (% Abs) is calculated using the TPSA values, which vary from 38.33 to 69.04 Å[25]. The compound's polarity and potential for water solubility are provided by TPSA. Lower TPSA values suggest that a compound is more polar and can interact with water molecules, improving its solubility in water. As a key indicator of a molecule's ability to penetrate cell membranes, log p is a measurement of a compound's partition coefficient between n-octanol and water. Greater lipophilicity is suggested by high Log p values, which may improve membrane permeability but also raise concerns about solubility and potential toxicity. The compound's potential for molecular interactions is estimated by the number of hydrogen bond donors and acceptors. Hydrogen bond donors and acceptors are crucial components in ligand-receptor interactions because they affect the compounds' binding affinity and specificity for their target. Additionally, the compound's flexibility is demonstrated by the number of rotatable bonds. In addition to potentially affecting the compounds' bioactivity, metabolism, and pharmacokinetic characteristics, a higher percentage of rotatable bonds can affect the compounds' conformational flexibility. Bioavailability radar provided by SwissADME presented that all designed compounds showed significant physicochemical features for appropriate oral bioavailability, and %ABS of all the designed chalcones varies from 85.18 to 95.77 %. Bioavailability radars for compounds 7B1, 7B2, 7B3, 9B2 and 9B3 were displayed in Fig. 11 (bioavailability radars for the remaining compounds are included in the supporting information). In the radar pink zone, all the designed compounds are present. Our investigation effectiveness depends on the estimation of ADME and toxicity risk[26]. The current study employs Osiris property exploration to identify the synthetic compounds' physicochemical properties, such as solubility and cLogP, which give the compounds their drug-like behaviour, as well as their undesirable toxicity threats, such as tumorigenicity, mutagenicity, irritation, and reproductive effects[27]. Despite the high risk of irritating behaviour for $7B_4$, $9B_1$ and $9B_2$, none of the other compounds ($7B_1$, $7B_2$, $7B_3$, $7B_5$, $7B_6$, $7B_7$ and $9B_3$) showed any toxicity risk. Computational analysis results for all the designed chalcones showed favourable pharmacokinetic characteristics.

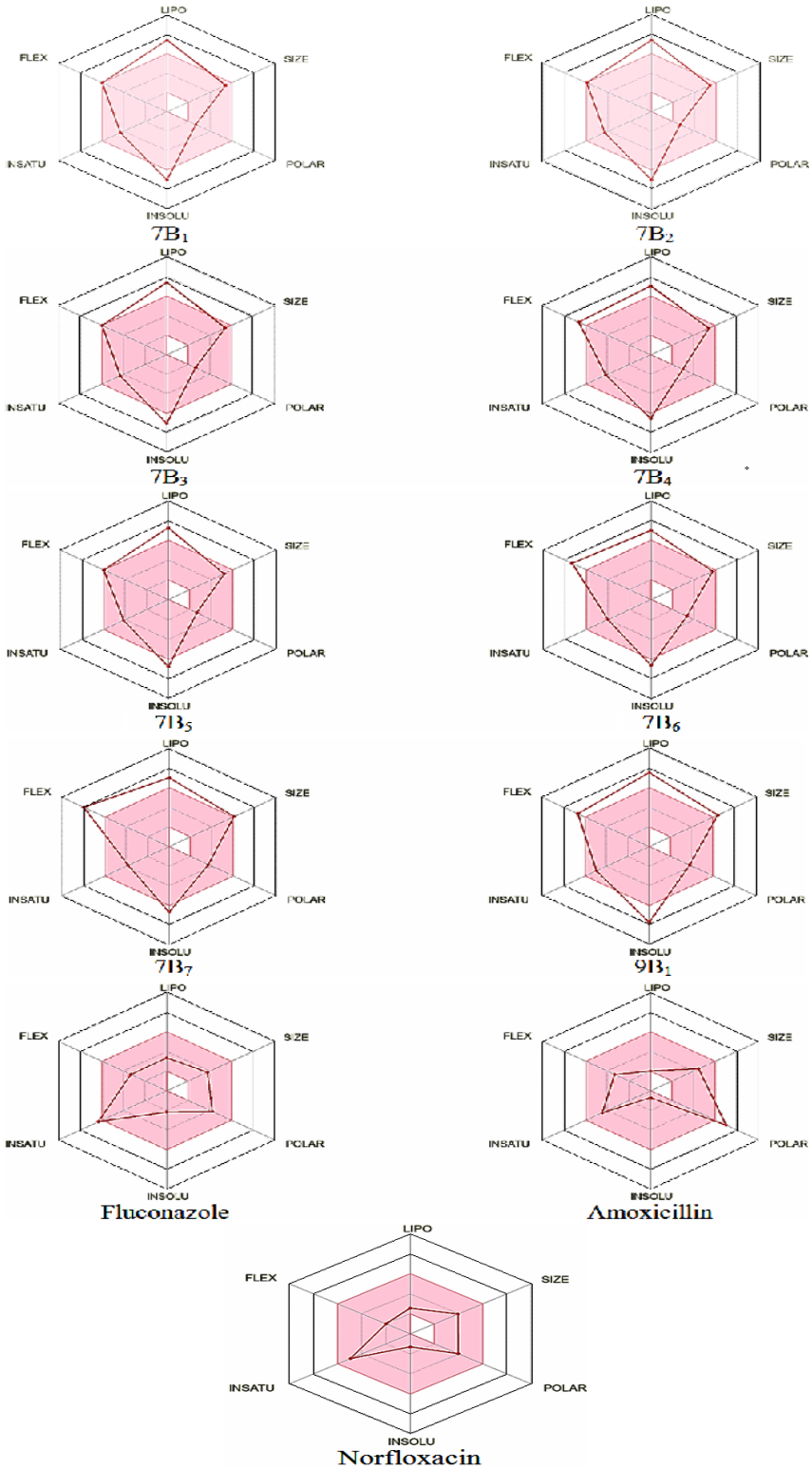

Fig. 11. A cursory comparison of test compounds $7B_1$-$7B_7$ and $9B_1$-$9B_3$ drug likeness characteristics of typical medications utilizing bioavailability radar. The optimal characteristics for oral bioavailability are presented in the pink coloured zone using SwissADME software

Table 3: Insilico ADMET screening for designed compounds

Parameters/Samples	$7B_1$	$7B_2$	$7B_3$	$7B_4$	$7B_5$	$7B_6$	$7B_7$	$9B_1$	$9B_2$	$9B_3$	Amoxicillin	Fluconazole	Norfloxacin
							Physicochemical Properties						
Molecular weight	452.03	452.03	452.03	447.61	431.61	477.63	507.66	534.69	534.69	534.69	365.40	306.27	319.34
Heavy atoms	32	32	32	33	32	35	37	40	40	40	25	22	23
Arm. heavy atoms	12	12	12	12	12	12	12	21	21	21	16	16	10
Fraction Csp3	0.46	0.46	0.46	0.48	0.48	0.5	0.52	0.38	0.38	0.38	0.44	0.23	0.38
Rotatable bonds (<10)	9	9	9	10	9	11	12	10	10	10	5	5	3
H-bond accepters (<7)	2	2	2	3	2	4	5	4	4	4	6	7	5
H-bond donors (<5)	1	1	1	1	1	1	1	1	1	1	4	1	2
Molar refractivity	134.59	134.59	134.59	136.07	134.54	142.56	149.05	162	162	162	94.59	70.71	92.55
TPSA (<90)	38.33	38.33	38.33	47.56	38.33	56.79	66.02	69.04	69.04	69.04	58.26	81.65	74.57
							Lipophilicity						
I LOG P	4.91	5.05	4.97	5.03	4.8	5.21	5.47	5.2	5.27	5.24	1.46	0.41	2.16
WLOG P	6.97	6.97	6.97	6.33	6.62	6.33	6.34	7.05	7.05	7.05	-0.68	1.47	0.93
MLOG P	4.84	4.84	4.84	3.99	4.57	3.62	3.27	5.08	5.08	5.08	0.23	1.47	1.01
SILICOS-IT	7.22	7.22	7.22	6.66	7.11	6.75	6.84	6.52	6.52	6.52	-0.45	0.71	1.82
Consensus Log P	6.28	6.31	6.29	5.76	6.07	5.74	5.74	6.31	6.32	6.32	-0.29	0.88	0.98
							Water Solubility						
(SILICOS-IT) Log S	-9.06	-9.06	-9.06	-8.58	-8.86	-8.68	-8.77	-10.19	-10.19	-10.19	-0.70	-3.54	-3.70
							Pharmacokinetics						
GI absorption	Low	Low	Low	High	High	High	High	Low	Low	Low	Low	High	High
BBB permeant	No	No	No	No	No	No	No	No	No	No	No	No	No
P-gp substrate	Yes	Yes	Yes	Yes	Yes	Yes	Yes	Yes	Yes	Yes	No	Yes	Yes
CYP2D6	Yes	Yes	Yes	Yes	Yes	Yes	Yes	Yes	Yes	Yes	No	No	No
CYP3A4	Yes	Yes	Yes	Yes	Yes	Yes	Yes	Yes	Yes	Yes	No	No	No
Log Kp (skin permeation)	-3.75	-3.75	-3.75	-4.19	-3.81	-4.39	-4.59	-4.09	-4.09	-4.09	-9.94	-7.92	-8.98
							Drug-likeness						
Drug-likeness	1.05	0.36	1.06	0.59	-1.16	2.52	3.51	-3.7	-4.14	-5.46	10.21	1.99	2.17
Lipinski	Yes;1 violation, MLOGP >4.15	Yes;1, violation MLOGP >4.15	Yes;1 violation, MLOGP >4.15	Yes; 0 violation	Yes; 1 violation, MLOGP >4.15	Yes; 0 violation	Yes; 1 violation: MW>500	Yes; 2 violations, MLOGP >4.15	Yes; 1 violation, MLOGP >4.15	Yes; 1 violation, MLOGP >4.15	Yes; 0 violation	Yes; 0 violation	Yes; 0 violation
Bioavailability	0.55	0.55	0.55	0.55	0.55	0.55	0.55	0.17	0.17	0.55	0.55	0.55	0.55
PAINS alert	0	0	0	0	0	0	0	0	0	0	0	0	0
Lead likeness violation	No; 3 violations: MW>350,	No; 3 violations: MW>350,	No; 3 violations: MW>350,	No; 3 violations: MW>350,	No; 3 violations: MW>350,	No; 3 violations: MW>350,	No; 3 violations: MW>350,	No; 3 violations: MW>350,	No; 3 violations: MW>350,	No; 3 violations: MW>350,	No; 1 violation: MW>350	No; 1 violation: MW>350	Yes

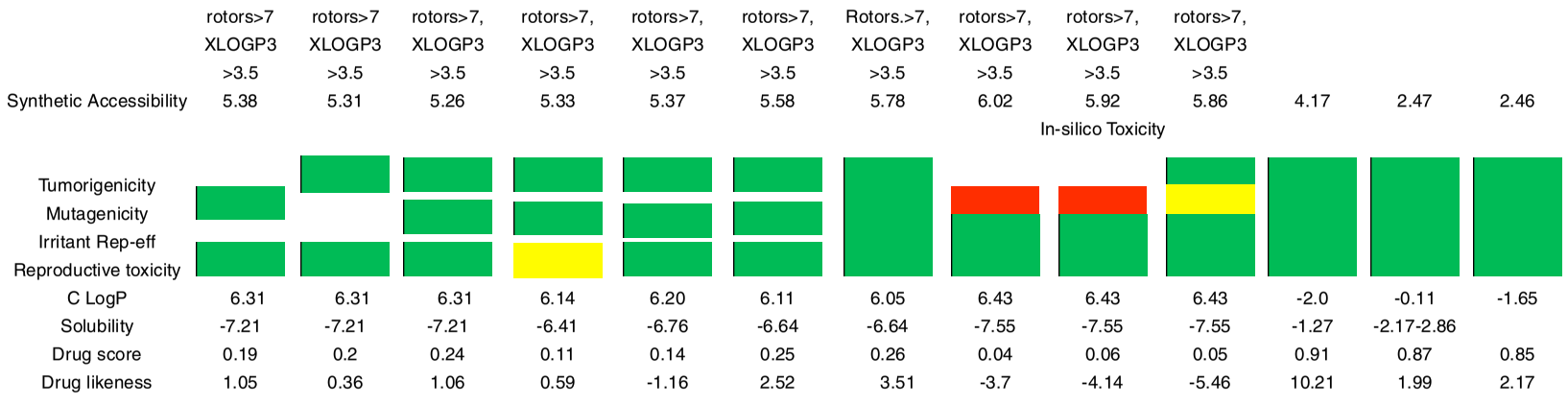

Note: Bioavailability score (0-1,1 better), Synthetic accessibility (1-10, lowest preferred), Drug-confirmed property (green), Moderate risk of toxicity (yellow), and High risk of toxicity (red).

Table 4: ADMET screening for similarity calculations

Compound Code	MW	MR	CAA	CMA	CSEB	OV	TPSA	DS	DL	C Log P	MiLogp	% Abs
7B1	452.03	134.59	767.919	422.304	397.272	1.6159	38.33	0.19	1.05	6.31	7.04	95.77
7B2	452.03	134.59	779.044	779.044	400.115	1.6278	38.33	0.2	0.36	6.31	7.24	95.77
7B3	452.03	134.59	779.055	427.463	400.124	1.6278	38.33	0.24	1.06	6.31	7.27	95.77
7B4	447.61	136.07	795.999	436.619	407.653	1.6421	47.56	0.11	0.59	6.14	6.65	92.59
7B5	431.61	134.54	785.839	431.36	402.586	1.6360	38.33	0.14	-1.16	6.20	7.04	95.77
7B6	477.63	142.56	828.173	457.955	430.38	1.6612	56.79	0.25	2.52	6.11	6.24	89.40
7B7	507.66	149.05	862.974	479.766	451.899	1.6846	66.02	0.26	3.51	6.05	6.22	86.22
9B1	534.69	162	863.53	484.915	455.76	1.6931	69.04	0.04	-3.7	6.43	7.26	85.18
9B2	534.69	162	889.972	495.685	460.978	1.71765	69.04	0.06	-4.14	6.43	7.27	85.18
9B3	534.69	162	889.989	495.699	460.992	1.7176	69.04	0.05	-5.46	6.43	7.08	85.18
Amoxicillin	365	94.59	599.80	332.63	345.634	1.39661	-2.0	158.26	10.21	0.91	-3.35	54.40
Norfloxacin	319	92.55	543.68	286.701	266.723	1.4307	-1.65	74.57	2.17	0.85	1.12	83.27
Fluconazole	306	70.71	599.80	332.63	345.63	1.13966	-0.11	81.65	1.99	0.87	-0.12	80.83

Similarity calculations

Utilizing six physicochemical constraints, the test compounds' physicochemical resemblance to reference drugs ($7B_1$-$7B_7$ and $9B_1$-$9B_3$) was predictable[28]. Table 5 shows the similarity results. Most consistent compounds strongly seem like the standard drug, notably $7B_1$ and $7B_5$.

Table 5: Similarity % of antimicrobial new chalcones with standard drugs

Compound code	Amoxicillin	Norfloxacin	Fluconazole
$7B_1$	73.10	58.55	71.23
$7B_2$	59.74	50.56	57.62
$7B_3$	72.35	57.61	51.30
$7B_4$	70.80	55.77	50.00
$7B_5$	72.53	57.89	51.96
$7B_6$	64.99	48.80	53.67
$7B_7$	58.98	41.77	57.10
$9B_1$	53.92	47.01	69.69
$9B_2$	52.34	45.09	68.48
$9B_3$	52.34	45.08	67.48

CONCLUSION

The terpenoid family includes a wide range of and β unsaturated flavonoid chalcone molecules with various biological properties. We created and verified a structure-based pharmacophore model to extract potent inhibitors of lanosterol α-demethylase and DNA gyrase topoisomerase B from our database of chalcones and their benzotriazole derivatives. By interacting with every residue of an important amino acid, the docking study proved that substituted benzaldehyde chalcone and their benzotriazole derivatives revealed better alignment at the active site. Consequently, this *in-silico* methodology helped identify the lead compounds and may help explain some of their positive effects during the in vivo study. Based on these investigations have recently shown that various compounds of the substituted benzaldehyde chalcone and related benzotriazole series displayed inhibitory effects on lanosterol α-demethylase and DNA gyrase topoisomerase B. The current study findings clearly showed that a reliable derivative of chalcones and their benzotriazole family may have intriguing antibacterial and antifungal properties. With their therapeutic potential, the compounds against (lanosterol α-demethylase, 4WMZ) 9B1, 9B2, 9B3, and 7B1 exhibit strong antifungal action, and (DNA gyrase topoisomerase B, 1KZN) 7B1, 7B2, and 9B2 exhibit strong antibacterial action and are possibly helpful as medications after more development. *In-silico* ADMET assessments enhance their potential as therapeutic agents by giving information on their pharmacokinetic characteristics, toxicity profiles, and drug-likeness. All factors considered the chalcone analogues offer an intriguing direction for further study and development with significant implications for therapeutic uses in biology and chemistry.

ACKNOWLEDGMENT

The authors thank to IFTM University Moradabad, Uttar Pradesh, India for providing laboratory and testing facilities for this research work.

Conflict of interest

The author declare that we have no conflict of interest.

REFERENCES

1. Rammohan, A; Reddy, J.S.; Sravya, G; Rao, C.N.; Zyryanov, G.V., *Environmental Chemistry Letters*., **2020**, 433-58.
2. Go, M.L.; Wu, X.; Liu, X.L., *Current Medicinal Chemistry*., **2005**, *12*(4), 483-99.
3. Sharma, D.; Kumar, S.; Narasimhan, B.; Ramasamy, K.; Lim, S.M.; Shah, S.A.; Mani, V., *BMC Chemistry*., **2019**, 1-4.
4. Rastogi, K.; Chang, J.Y.; Pan, W.Y.; Chen, C.H.; Chou, T.C.; Chen, L.T.; Su, T.L., *Journal of Medicinal Chemistry*., **2002**, 4485-93.
5. Hilmy, K.M.; Kishk, F.N.; Shahen, E.B.; Sobh, E.A.; Hawata, M.A., *Drug Development Research*., **2023**, 1204-30.
6. Negi, A.; Pant, P.; Mathpal, S.; Tewari, D.; Upadhyay, S.K.; Chandra, S.; Kumar, R., *Indian Journal of Microbiology*., **2024**, 1-9.
7. Tratrat, C.; Haroun, M.; Xenikakis, I.; Liaras, K.; Tsolaki, E.; Eleftheriou, P.; Petrou, A.; Aldhubiab, B.; Attimarad, M.; Venugopala, K.N.; Harsha, S., *Current Topics in Medicinal Chemistry*., **2019**, 356-75.
8. Yadav, P.; Lal, K.; Kumar, A., *Drug Research*., **2021**, *71*(03), 149-56.
9. Doan, N.Q.; Tran, H.N.; Nguyen, N.T.; Pham, T.M.; Nguyen, Q.D.; Vu, T.T., *Chemistry & Biodiversity*., **2024**, *202*, 401142.
10. Mekheimer, R.A.; Abuo-Rahma, G.E.; Abd-Elmonem, M.; Yahia, R.; Hisham, M.; Hayallah, A.M.; Mostafa, S.M.; Abo-Elsoud, F.A.; Sadek, K.U., *Journal of Molecular Structure*., **2022**, *13*, 3615.

11. Soni, J; Sahiba, N; Sethiya, A.; Teli, P.; Agarwal, D.K.; Manhas, A.; Jha, P.C.; Joshi, D.; Agarwal, S., *Polycyclic Aromatic Compounds*., **2022**, *29*, 70-90.
12. Nippu, B.N.; Sharma, G.C.; Jangir, M.; Sharma, A.; Chauhan, N.S., *Results in Chemistry*., **2024**, *10*, 1662.
13. Savaspun, K.; Boonchaisri, S.; Chaisuriya, P.; Srisomsap, C.; Svasti, J.; Ardkhean, R.; Phanumartwiwath, A.; Sam-ang, P., *Science Asia*., **2023**, *49*(3).
14. Ahsan, R.; Paul, S.; Alam, M.S.; Rahman, A.M., *ACS Omega*., **2025**.
15. Rocha, J.E.; de Freitas, T.S.; da Cunha Xavier J.; Pereira, R.L.; Junior, F.N.; Nogueira, C.E.; Marinho, M.M.; Bandeira, P.N.; de Oliveira, M.R.; Marinho, E.S.; Teixeira, A.M., *Biomedicine & Pharmacotherapy.,* **2021**, *140*, 111768.
16. Dadou, S.; Altay, A.; Koudad, M.; Türkmenoğlu, B.; Yeniçeri, E.; Çadır, S.; Allali, M.; Oussaid, A.; Benchat, N.; Karrouchi, K., *Medicinal Chemistry Research*., **2022**, *13*, 69-83.
17. Subramanian, G.; Rajagopal, K.; Sherin, F., *Research Journal of Pharmacy and Technology*., **2020**, *27*, 08-14.
18. Suriyakala, T.; Ravindran, G.U., *Oriental Journal of Chemistry*., **2022**, *38*(5), 1250.
19. Karale, B.K.; Takate, S.J.; Salve, S.P.; Zaware, B.H.; Jadhav, S.S., Orient. J. Chem., *201*, 307-15.
20. Kumar, S.; Wahi, A.K.; Singh, R. *European J. Medicinal Chemistry*., **2011**, *46*(9), 4753-9.
21. Liu, H.; Gopala, L.; Avula, S.R.; Jayakumar, P.; Peng, X.; Zhou, C.; Geng, R., *Chinese Journal of Chemistry*., **2017**, *4,* 83-96.
22. Wang, X.L.; Wan, K.; Zhou, C.H., *European J. Medicinal Chemistry*., **2010**, *46*, 31-9.
23. Patil, S; Randive, V.; Mahadik, I.; Asgaonkar, K., *Current Drug Disco. Technol.* **2024**, 9-19.
24. da Cunha Xavier, J.; de Queiroz Almeida-Neto, F.W.; da Silva, P.T.; de Sousa, A.P.; Marinho, E.S.; Marinho, M.M.; Rocha, J.E.; Freitas, P.R.; de Araújo, A.C.; Freitas, T.S.; Nogueira, C.E., *Journal of Molecular Structure*., **2021**, *1227*, 129692.
25. Ibrahim, T.S.; Almalki, A.J.; Moustafa, A.H.; Allam, R.M.; Abuo-Rahma, G.E.; El Subbagh, H.I.; Mohamed, M.F., *Bioorganic Chemistry*., **2021**, *10*, 4885.
26. Mohanty, M.; Mohanty, P.S. Monatshefte, Für., *Chemie-Chemical Monthly*., **2023**, 683-707.
27. Nanjundaswamy, S.; Hema, M.K.; Karthik, C.S.; Rajabathar, J.R.; Arokiyaraj, S.; Lokanath, N.K.; Mallu, P., *Journal of Molecular Structure*., **2022**, *1247*, 131365.
28. Kumar, S.; Wahi, A.K.; Singh, R., *Arabian Journal of Chemistry*., **2016**, S1450-6.